

Ethmoidectomy Combined with Superior Meatus Enlargement Increases Olfactory Airflow

Hironobu Nishijima, MD; Kenji Kondo, MD, PhD; Tsutomu Nomura, MD, PhD; and
Tatsuya Yamasoba, MD, PhD

Objectives: The relationship between a particular surgical technique in endoscopic sinus surgery (ESS) and airflow changes in the post-operative olfactory region has not been assessed. The present study aimed to compare olfactory airflow after ESS between conventional ethmoidectomy and ethmoidectomy with superior meatus enlargement, using virtual ESS and computational fluid dynamics (CFD) analysis.

Study Design: Prospective computational study.

Materials and Methods: Nasal computed tomography images of four adult subjects were used to generate models of the nasal airway. The original preoperative model was digitally edited as virtual ESS by performing uncinectomy, ethmoidectomy, antrostomy, and frontal sinusotomy. The following two post-operative models were prepared: conventional ethmoidectomy with normal superior meatus (ESS model) and ethmoidectomy with superior meatus enlargement (ESS-SM model). The calculated three-dimensional nasal geometries were confirmed using virtual endoscopy to ensure that they corresponded to the post-operative anatomy observed in the clinical setting. Steady-state, laminar, inspiratory airflow was simulated, and the velocity, streamline, and mass flow rate in the olfactory region were compared among the preoperative and two postoperative models.

Results: The mean velocity in the olfactory region, number of streamlines bound to the olfactory region, and mass flow rate were higher in the ESS-SM model than in the other models.

Conclusion: We successfully used an innovative approach involving virtual ESS, virtual endoscopy, and CFD to assess postoperative outcomes after ESS. It is hypothesized that the increased airflow to the olfactory fossa achieved with ESS-SM may lead to improved olfactory function; however, further studies are required.

Key Words: virtual endoscopic sinus surgery, computational fluid dynamics, virtual endoscopy, olfactory airflow, olfaction.

Level of Evidence: NA.

INTRODUCTION

Endoscopic sinus surgery (ESS) is the primary surgical treatment for chronic rhinosinusitis that is refractory to medical treatment. The primary aim of ESS is to resolve mucosal inflammation by improving drainage and

ventilation of affected sinuses. A number of previous studies have demonstrated that ESS can improve postoperative olfactory function.^{1,2} In cases of chronic rhinosinusitis with nasal polyposis, the main cause of olfactory loss is conduction block of the odorant, as polyps in the nasal passage prevent the odorant from reaching the olfactory neuroepithelium. Therefore, a surgical technique to regain postoperative airflow in the olfactory region might improve the postoperative olfactory outcome.

Few studies have suggested a relationship between a particular surgical technique in ESS and postoperative olfactory function.³ In particular, the importance of superior meatus enlargement combined with ethmoidectomy for improving post-operative olfaction has been stressed. Miwa et al. reported that the middle turbinate fenestration method, which is similar to ethmoidectomy combined with superior meatus enlargement, results in good improvement of the postoperative olfactory threshold, suggesting that this surgical technique may effectively increase olfactory airflow.³ However, information regarding the change in olfactory airflow after ESS remains limited.⁴ It is difficult to intuitively predict the postoperative changes in invisible olfactory airflow, owing to the complex structures in the ethmoid region of the sino-nasal cavity. Therefore, selecting a particular surgical technique to improve olfactory function in ESS is primarily based on the personal experience of the surgeon.

This is an open access article under the terms of the Creative Commons Attribution-NonCommercial-NoDerivs License, which permits use and distribution in any medium, provided the original work is properly cited, the use is non-commercial and no modifications or adaptations are made.

Additional Supporting Information may be found in the online version of this article.

From the Department of Otolaryngology (H.N., K.K., T.Y.), The University of Tokyo, Tokyo, Japan; and the Department of Otolaryngology (T.N.), Saitama Medical Center, Saitama Medical University, Saitama, Japan

Editor's Note: This Manuscript was accepted for publication 10 November 2016.

Sources of Financial Support or Funding: This work was supported by a JFE (The Japanese Foundation for Research and Promotion of Endoscopy) Grant, JSPS KAKENHI Grant Numbers JP26293366 and JP24592586, Grants-in-aid for Scientific Research from the Japanese Ministry of Health, Labour and Welfare (H26- H27-research on measures for intractable disease-general-, and the Practical Research Project for Rare/Intractable Diseases from the Japan Agency for Medical Research and Development (AMED).

Conflict of Interest: No conflict of interest exists.

Send correspondence to Hironobu Nishijima, MD, Department of Otolaryngology, The University of Tokyo, 7-3-1 Hongo Bunkyo-ku, Tokyo 113-8655, Japan. Email: nishijimahironobu@gmail.com

DOI: 10.1002/liv.2.59

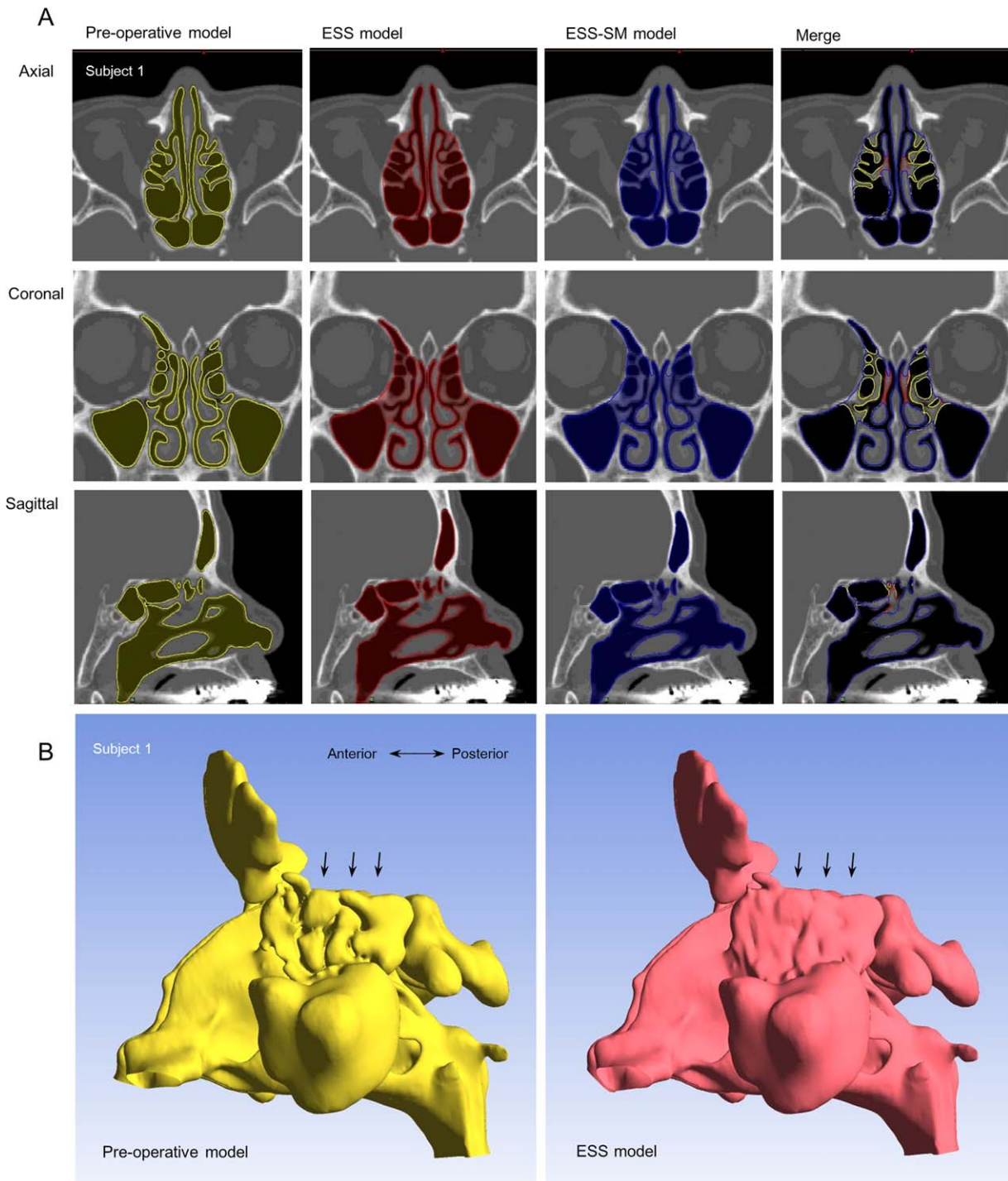


Fig. 1. Virtual Surgery. A) Morphology editing using Mimics. The preoperative model (yellow), endoscopic sinus surgery (ESS) that included ethmoidectomy with normal superior meatus model (ESS model; red), and ESS that included ethmoidectomy with superior meatus enlargement model (ESS-SM model; blue), and a merged photograph of the contours of all the models at the same level of the axial, coronal, and sagittal planes are presented. The colored area is the geometry after the operation. B) Three-dimensional geometry of the nasal cavity in the pre-operative and ESS models. The black arrow indicates the area of the ethmoid sinus where virtual surgery was performed. The ethmoid sinus became one cavity after virtual ESS.

The method of computational fluid dynamics (CFD) allows the simulating of airflow using a computer. CFD techniques enable detailed prediction of airflow throughout the nasal cavity based on three-dimensional (3D) models derived from image data.⁵ The nasal

geometry of image data can be virtually modified with virtual surgery in a manner that reflects surgical changes, and new CFD simulations can be performed to determine the effect of virtual surgery.^{6,7} Nasal CFD and virtual surgery have been especially used to address the

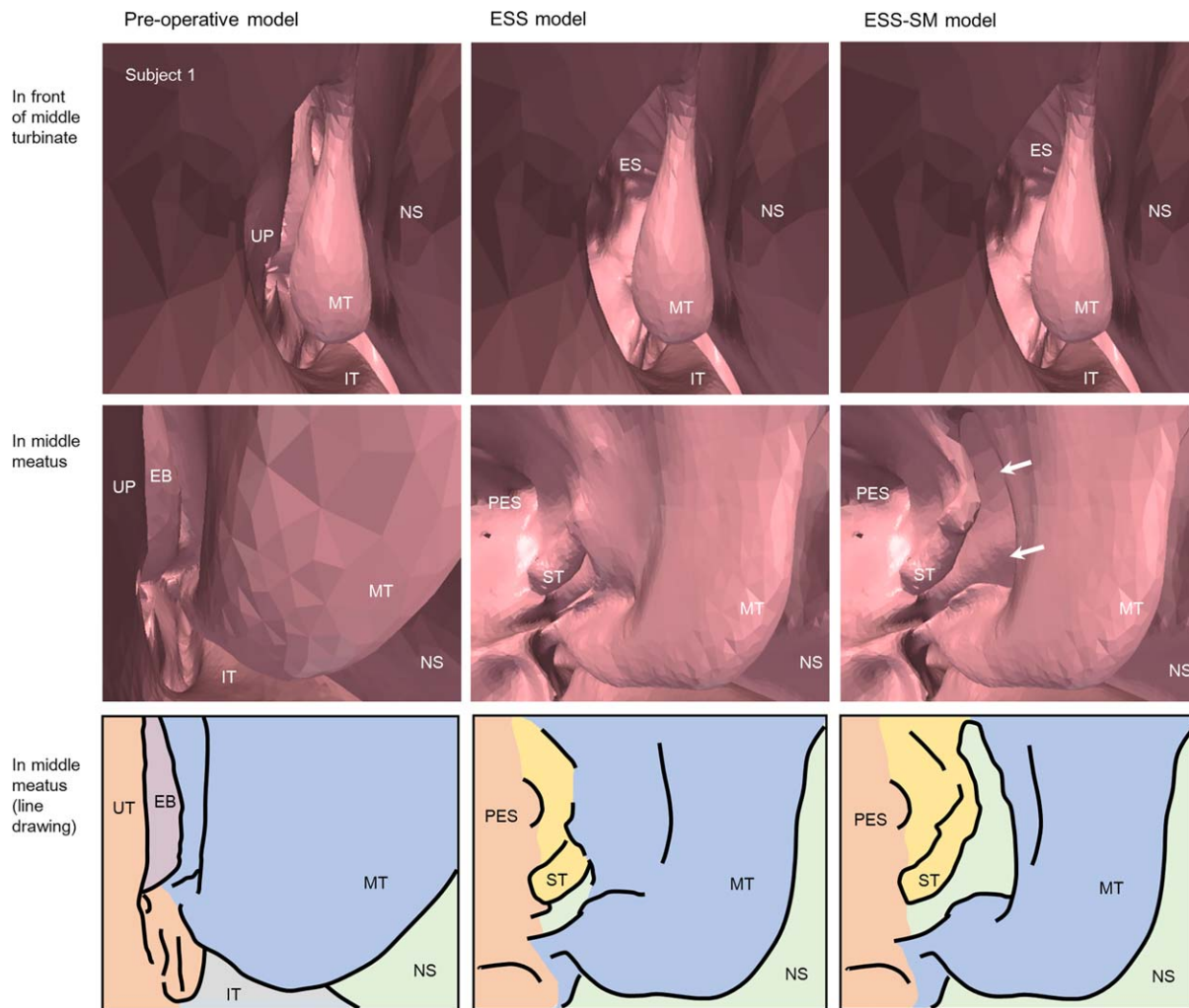


Fig. 2. Virtual Endoscopy at the Right of the Nasal Cavity. Virtual endoscopy in the preoperative model, endoscopic sinus surgery (ESS) that included ethmoidectomy with normal superior meatus model (ESS model), and ESS that included ethmoidectomy with superior meatus enlargement model (ESS-SM model) in front of the middle turbinate and in the middle meatus. The white arrows indicate superior meatus enlargement. The entire superior turbinate could be observed from the middle meatus in the ESS-SM model. MT, middle turbinate; IT, inferior turbinate; NS, nasal septum; UP, uncinate process; EB, ethmoidal bulla; ST, superior turbinate; PES, posterior ethmoid sinus.

issue of nasal airway obstruction.^{6–11} One of the potential difficulties for the application of CFD in the olfactory region after virtual ESS is complicated editing of the ethmoid region in the image data using two-dimensional (2D) editing techniques. Because of the complex structures in the ethmoid region, it is sometimes difficult to confirm whether the 3D nasal geometry structured from 2D editing actually corresponds well with the nasal anatomy after ESS.

In the present study, we aimed to compare olfactory airflow between conventional ethmoidectomy and ethmoidectomy with superior meatus enlargement using virtual ESS and computational fluid dynamics analysis in order to determine the relationship between a particular surgical technique in ESS and airflow changes in the postoperative olfactory region. In order to overcome the difficulty of corresponding the 2D-edited nasal geometry to the predicted nasal anatomy after ESS, we introduced new virtual endoscopy techniques.

MATERIALS AND METHODS

Subjects

The first study included four adults (one male and three female subjects; age range, 37–75 years) without lesions associated with sinus diseases or severe nasal septal deviation. The subjects were sequentially numbered from 1 to 4. These subjects visited our outpatient clinic with the complaint of post-nasal drip. Computed tomography (CT) studies were performed to screen for latent sinus diseases; however, no abnormalities were identified. The nasal structures and mucosa in all the subjects were normal on nasal inspection. We then studied two cases of chronic sinusitis. In these patients, nasal endoscopy revealed multiple nasal polyps in the olfactory cleft and middle meatus. The patients complained of smell loss, which fluctuated depending on the steroid intake, and it was compatible with conductive smell loss by airflow blocking. All procedures were performed in accordance with the guidelines of the University of Tokyo, and the study was approved by the institutional review board (approval no. 2487).

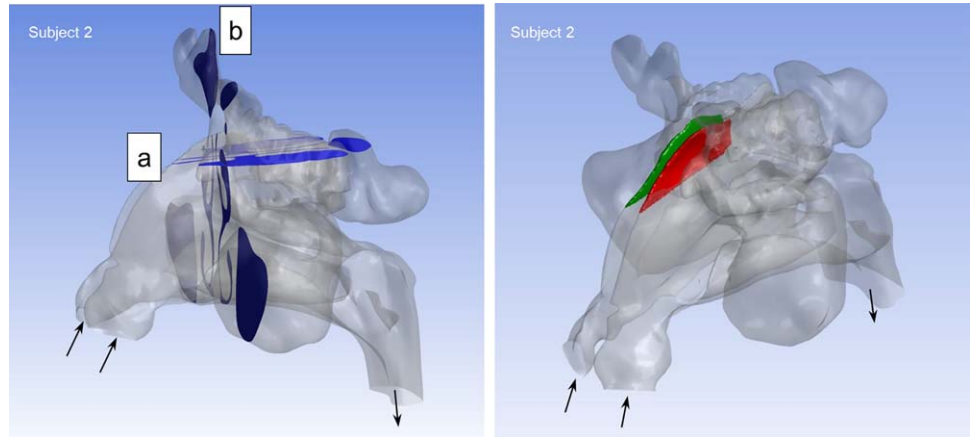


Fig. 3. Evaluated Area in the Nasal Cavity. The nasal cavity model constructed from computed tomography images. A) Axial plane crossing the olfactory region. B) Coronal plane crossing the olfactory region. The solid olfactory region where quantitative analyses of velocity were performed is indicated in green (right side) and red (left side). The black arrows indicate the direction of airflow.

Virtual Surgery and Virtual Endoscopy

Postoperative models were created for each subject, using the original CT scan images with 0.8-mm-thick slices and the image analysis software Mimics 16.0 (Materialise NV, Leuven, Belgium). Virtual surgery was performed by hand-editing the anatomical structures in the 2D images using Mimics software to reproduce surgical changes. The procedures included uncinectomy, ethmoidectomy, anrostomy, and frontal sinusotomy. In anrostomy and frontal sinusotomy, each sinus ostium was widened as much as possible. In ethmoidectomy, an attempt was made to include all ethmoid cells into one cavity. The following two post-operative models were prepared: 1) ESS that included ethmoidectomy with a normal superior meatus (ESS model) and 2) ESS that included ethmoidectomy with superior meatus enlargement (ESS-SM model) (Fig. 1A). In the ESS-SM model, the basal lamella and adjacent part of the middle turbinate were removed almost 1 cm in front of the anterior aspect of the superior turbinate, enlarging the superior meatus in the anterior direction (Fig. 1A). The superior turbinate was kept intact.

To overcome the difficulties associated with virtual ESS, a new virtual endoscopic technique was developed using the ParaView software (Kitware Inc., Clifton Park, NY). This technique enabled the observation of the nasal cavity model in an endoscopic view, which is familiar to rhinologists and therefore makes virtual ESS easy to perform.

After 2D image editing, 3D reconstructions of the nasal cavity were created in 3D surface files (.stl) using Mimics software (Fig. 1B). These 3D nasal models were checked with virtual endoscopy using ParaView 5.0 to determine whether virtual surgery based on the 2D image editing reproduced the predicted post-operative status (Fig. 2, Supporting Video 1-3).

CFD Workflow

The geometry was meshed using ICEM-CFD 14.5 (ANSYS, Inc., Canonsburg, PA), and the numerical simulation was performed using ANSYS CFX 14.5 (ANSYS, Inc.). The models included about 2 million tetrahedral grids, and this number was thought to be sufficient to resolve the relative change tendency of the flow fields in the nasal cavity.¹² A finer prism layer was created near the mucosal surface to accurately resolve the rapidly changing near-wall air velocity profile.¹³

The CFD airflow simulation was performed under laminar, steady-state airflow and at a temperature of 20°C in the inspiratory direction. The boundary conditions to determine airflow were as follows, based on previous studies.^{7,8,14-16} The nasal walls were assumed to be a non-slip, rigid model. For the pressure-inlet condition at the nostrils, the gauge pressure was set to zero. For the pressure-outlet condition at the outlet, the gauge pressure was set

to negative, corresponding to a target steady-state flow rate. The target steady-state inspiratory airflow rate ranged from 13.2 L/min to 18.1 L/min (mean, 14.8 L/min). This flow rate represents an estimate of twice the patient's minute volume based on allometric scaling according to body weight.¹⁶

Outcome Measures

The aerodynamic parameters, including airflow velocity magnitude, airflow streamlines, which trace the airflow patterns with neutrally buoyant particles, and mass flow rate, were obtained using ANSYS CFX. These aerodynamic parameters were compared among the pre-operative and two post-operative models in the axial and coronal planes through the olfactory region (Fig. 3). The solid olfactory region was identified and extracted from the body of the nasal cavity using ANSYS Fluent 14.5 (ANSYS, Inc.), according to previous anatomical studies (Fig. 3).^{13,17,18} The mean and maximum velocities were calculated in the right and left sides of the solid olfactory region, respectively.

Statistical Analysis

Tukey's test was used for multiple comparisons. All statistical analyses were performed using StatFlex Ver. 6 (Artech Co., Ltd., Osaka, Japan). The level of significance was set at $P < 0.05$.

RESULTS

Velocity Changes in the Olfactory Region After Virtual ESS

To evaluate the changes in airflow in the olfactory region, we first analyzed the velocity magnitude in the preoperative and two postoperative models. The contour plots of the velocity of the preoperative and two postoperative models in the same plane are shown in Figure 4A. The velocity in the olfactory region was higher in the ESS-SM model than in the preoperative and ESS models (Fig. 4A). Quantitative analyses revealed that the mean postoperative velocity in the olfactory region was significantly greater in the ESS-SM model than in the preoperative and ESS models, and that the mean postoperative velocity in the olfactory region was not significantly different between the preoperative and ESS models (Fig. 4B).

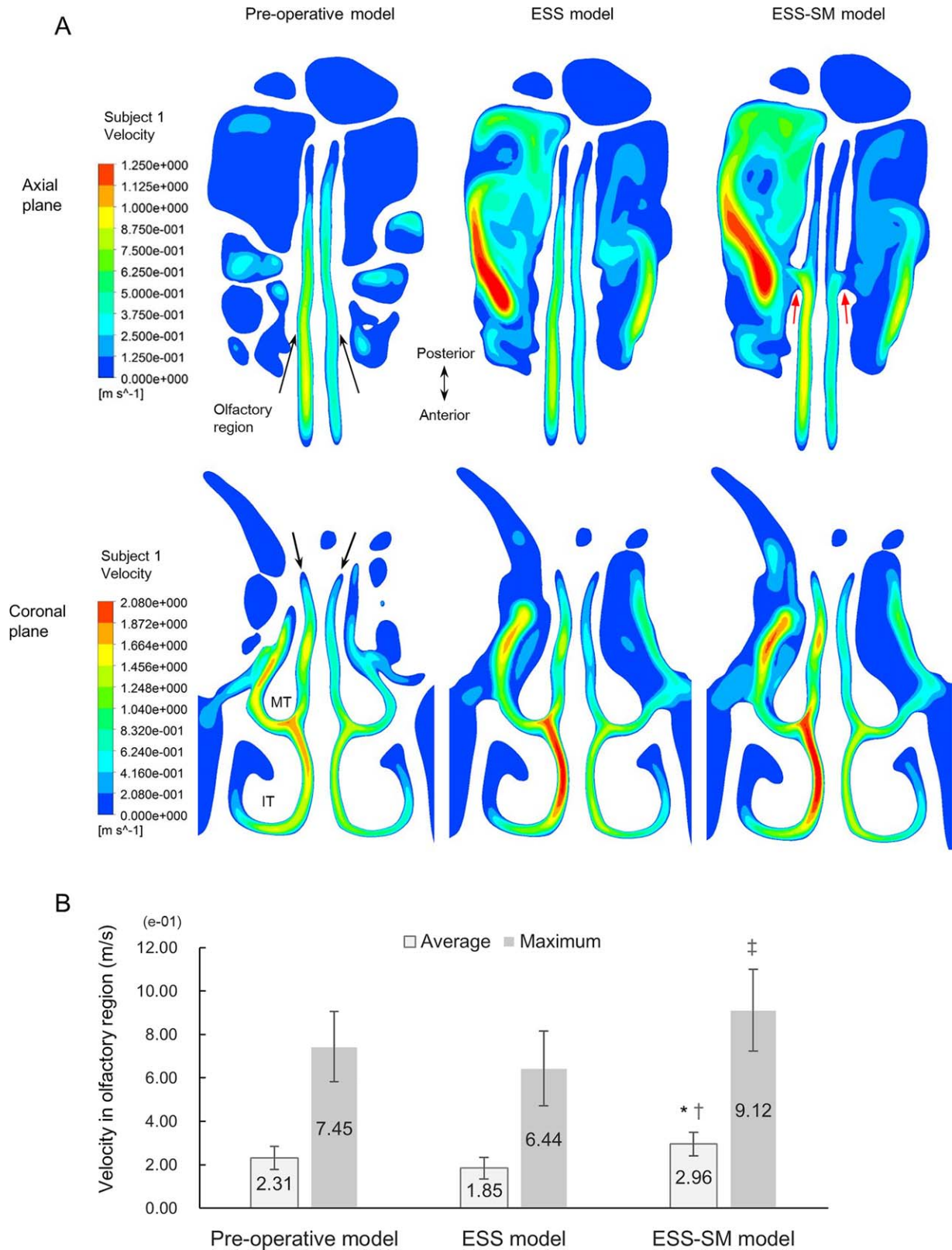


Fig. 4. Airflow Velocity in the Olfactory Region. A) Velocity in the pre-operative model, endoscopic sinus surgery (ESS) that included ethmoidectomy with normal superior meatus model (ESS model), and ESS that included ethmoidectomy with superior meatus enlargement model (ESS-SM model) in the axial and coronal planes. The black arrows indicate the olfactory region. The red arrows indicate superior meatus enlargement. Velocity around the olfactory region increased in the ESS-SM model. MT, middle turbinate; IT, inferior turbinate B) Comparison of the mean and maximum velocities in the olfactory region. *P < 0.05 vs. the pre-operative model, †P < 0.01 vs. the ESS model, ‡P < 0.05 vs. the ESS model (Tukey's test).

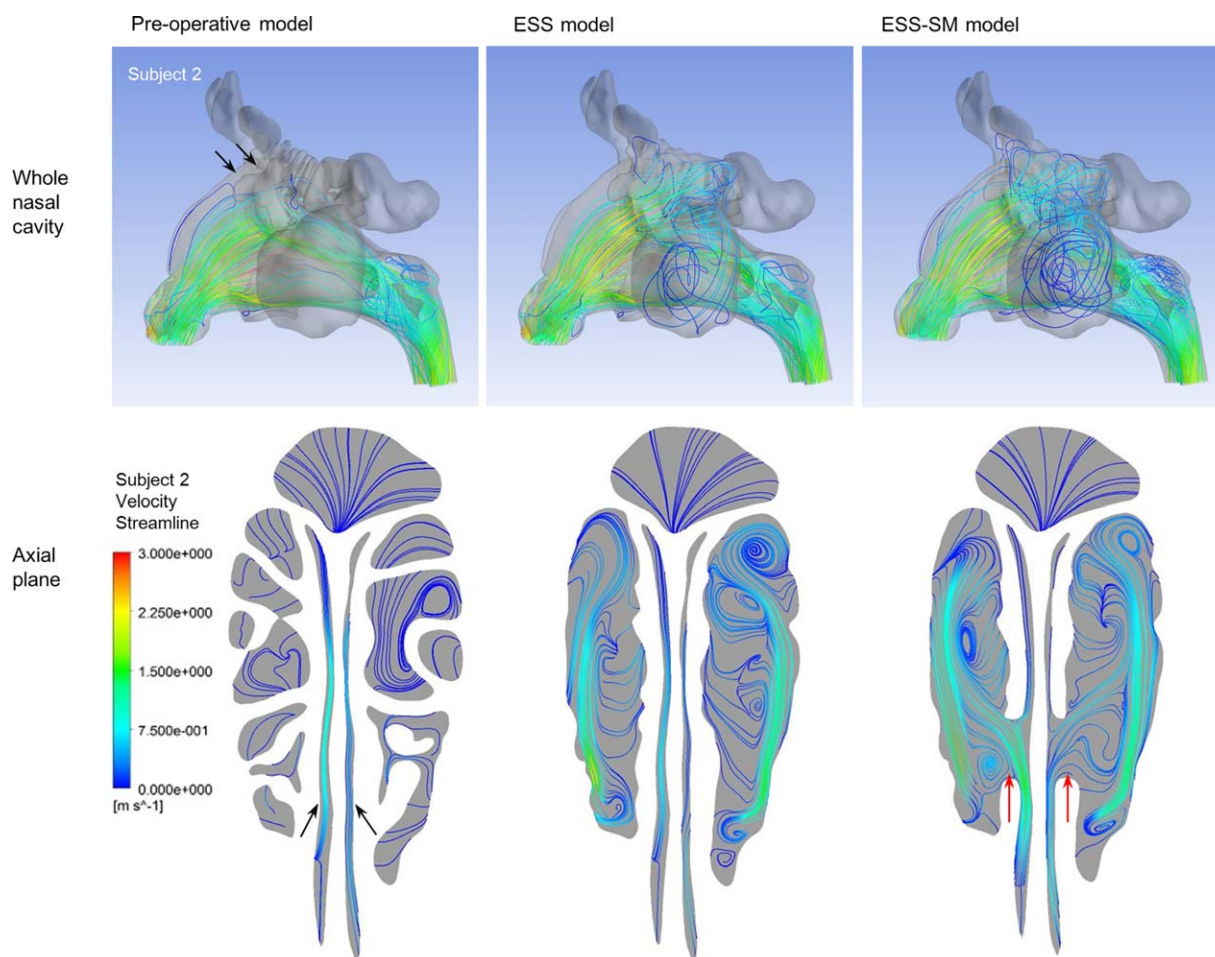


Fig. 5. Streamline in the Olfactory Region. Streamline in the pre-operative model, endoscopic sinus surgery (ESS) that included ethmoidectomy with normal superior meatus model (ESS model), and ESS that included ethmoidectomy with superior meatus enlargement model (ESS-SM model) in the entire nasal cavity and axial plane. The black arrows indicate the olfactory region. The red arrows indicate the airflow that passed from the superior meatus to the middle meatus. The streamline around the olfactory region is higher in the ESS-SM model than in the other models.

Streamline Changes in the Olfactory Region After Virtual ESS

To evaluate the changes in the airflow stream in the olfactory region following virtual ESS, we analyzed the streamline in the preoperative and two postoperative models. In the preoperative and ESS models, streamline analysis revealed that air passed through the olfactory region from the anterior opening to the posterior opening of the olfactory cleft, in a simple anteroposterior direction. However, in the ESS-SM model, air passed through the olfactory region from the enlarged superior meatus to the middle meatus, increasing the number of streamlines bound to the olfactory region (Fig. 5).

Mass Flow Rate Changes in the Olfactory Region

To evaluate the amount of airflow in the olfactory region after ESS, we analyzed the mass flow rate in the preoperative and two postoperative models. The mass flow rate in the olfactory region was higher in the

ESS-SM model than in the preoperative and ESS models (Fig. 6). Axial plane analysis of the olfactory region identified airflow in the upward direction (Fig. 6; indicated in green, yellow, and red) and downward direction (indicated in blue). The mass flow rates in both directions were higher in the ESS-SM model than in the ESS model.

Virtual ESS for Chronic Sinusitis Patients

To evaluate the changes in airflow after ESS in the olfactory region in patients with chronic sinusitis, we performed virtual ESS and ESS-SM in the patients with nasal polyps and compared the airflow parameters in the preoperative and two postoperative models. 3D reconstructions of the nasal cavity showed the absence of the nasal passage in most parts of the ethmoid region in the preoperative model, corresponding to occlusion of the region by nasal polyps and mucosal swelling (Fig. 7A). The contour plots of the velocity revealed that the velocity in the olfactory region increased after virtual surgery, especially after ESS-SM (Fig. 7B). Streamline

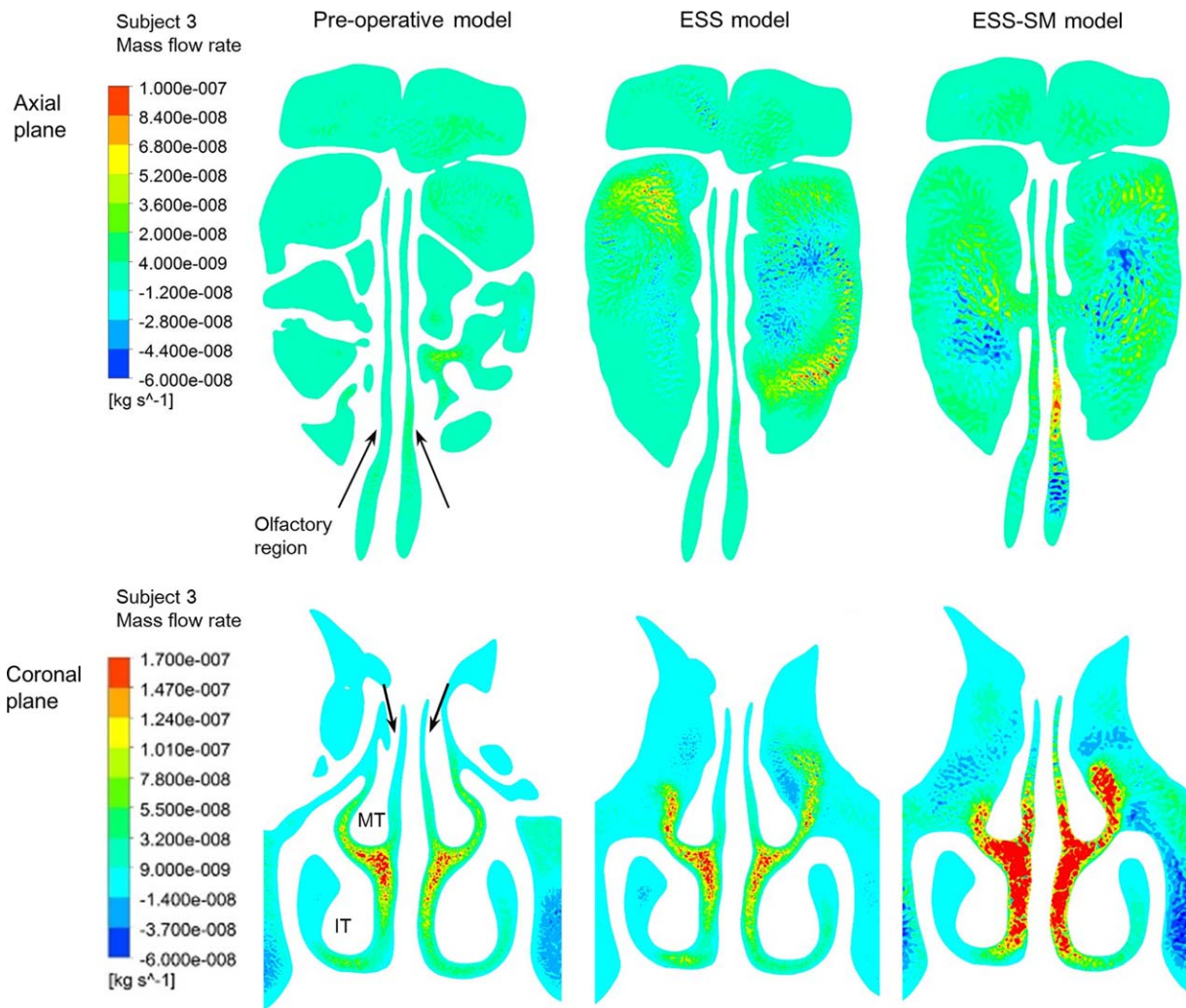


Fig. 6. Mass Flow Rate in the Olfactory Region. The mass flow rate in the preoperative model, endoscopic sinus surgery (ESS) that included ethmoidectomy with normal superior meatus model (ESS model), and ESS that included ethmoidectomy with superior meatus enlargement model (ESS-SM model) in the axial and coronal planes. The black arrows indicate the olfactory region. Axial plane analysis identified airflow in the upward direction (green, yellow, and red) and downward direction (blue). The mass flow rate in both directions is higher in the ESS-SM model than in the ESS model. MT = middle turbinate; IT = inferior turbinate.

analysis revealed that the number of streamlines bound to the olfactory region increased after virtual surgery. In the ESS-SM model (Fig. 8A), air flow was found to pass through the olfactory region from the enlarged superior meatus to the middle meatus. Mass flow rate analysis also showed increased mass flow after virtual surgery, especially after ESS-SM (Fig. 8B). These findings indicate that both ESS and ESS-SM may lead to increased olfactory airflow in cases of chronic sinusitis. Furthermore, when compared between ESS and ESS-SM, the olfactory airflow indicated by velocity, streamlines, and mass flow rate was higher in the ESS-SM model than in the ESS model.

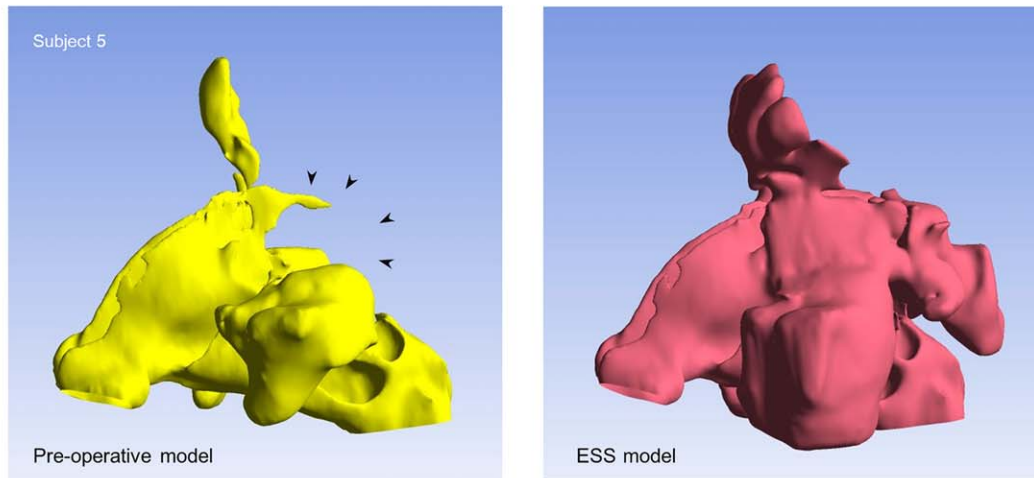
DISCUSSION

The novel finding in our simulation of nasal airflow using CFD is that the velocity, streamlines, and mass flow rate in the olfactory region were better increased

with ESS-SM than with conventional ESS. The velocity and streamline profiles in numerical simulations have been widely used to indicate the airflow status in the olfactory region.^{19–21} The increase in these parameters suggests that the amount of airflow through the olfactory region increases after superior meatus enlargement. Our findings support the findings of a previous report, which showed that a surgical method similar to ESS-SM resulted in good improvement of the postoperative olfactory threshold.³

The possible reason for the increase in the airflow of the olfactory region in the ESS-SM model is that the enlarged superior meatus reduced the airflow resistance through the olfactory cleft. This was actually demonstrated by streamline analysis, in which some of the inspired airflow passed through the olfactory region and exited from the enlarged superior meatus to the middle meatus, increasing the number of streamlines bound to the olfactory region in the ESS-SM model (Fig. 5).

A



B

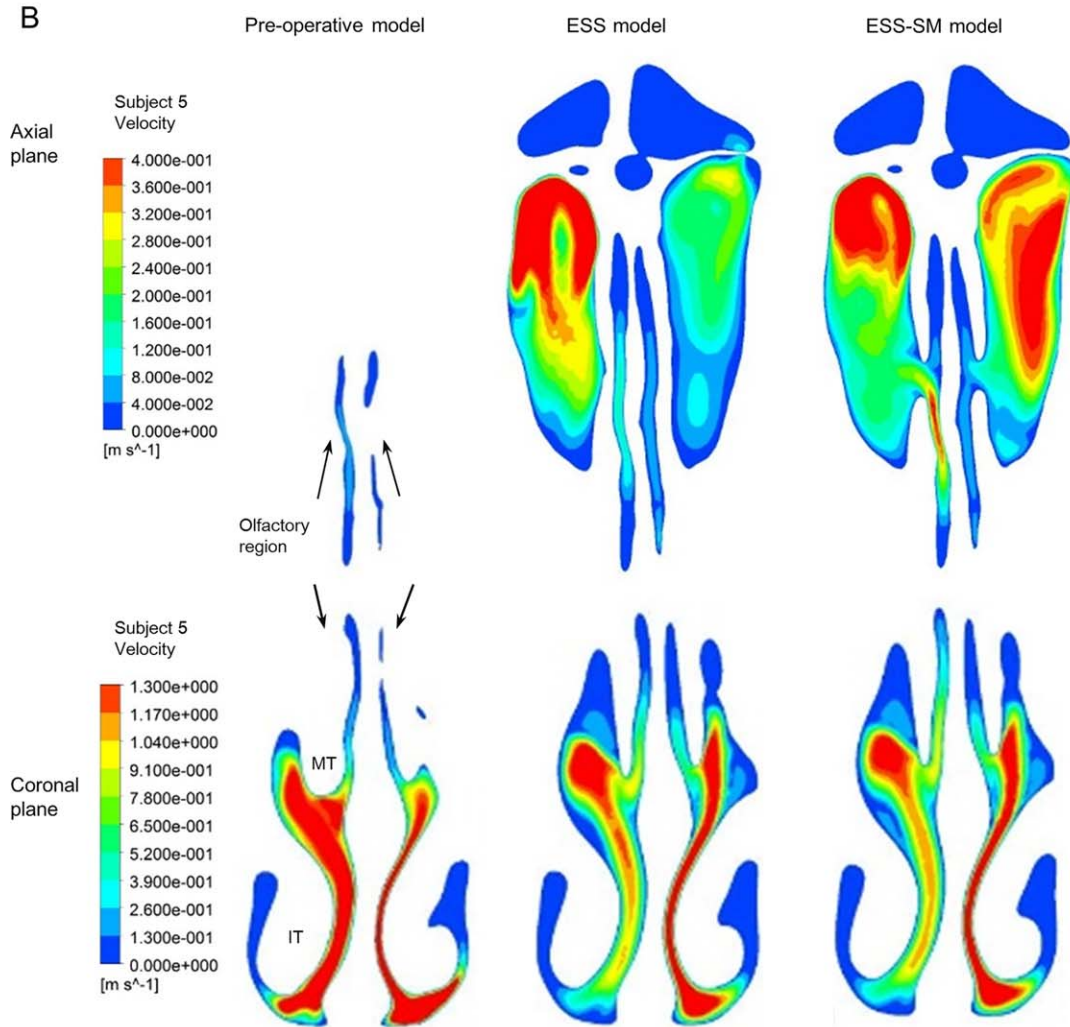


Fig. 7. Airflow Velocity in the Olfactory Region of Chronic Sinusitis Patients. A) Three-dimensional geometry of the nasal cavity in the pre-operative model and endoscopic sinus surgery (ESS) that included ethmoidectomy with normal superior meatus model (ESS model). The black arrowheads indicate the area of the ethmoid sinus and olfactory cleft where the nasal passage was absent due to nasal polyps, and virtual surgery was performed. The ethmoid sinus replaced nasal polyps with an air passage, becoming one cavity after virtual ESS. B) Velocity in the preoperative model, ESS model, and ESS that included ethmoidectomy with superior meatus enlargement model (ESS-SM model) in the axial and coronal planes. The black arrows indicate the olfactory region. Velocity around the olfactory region increased in the ESS-SM model. MT = middle turbinate; IT = inferior turbinate.

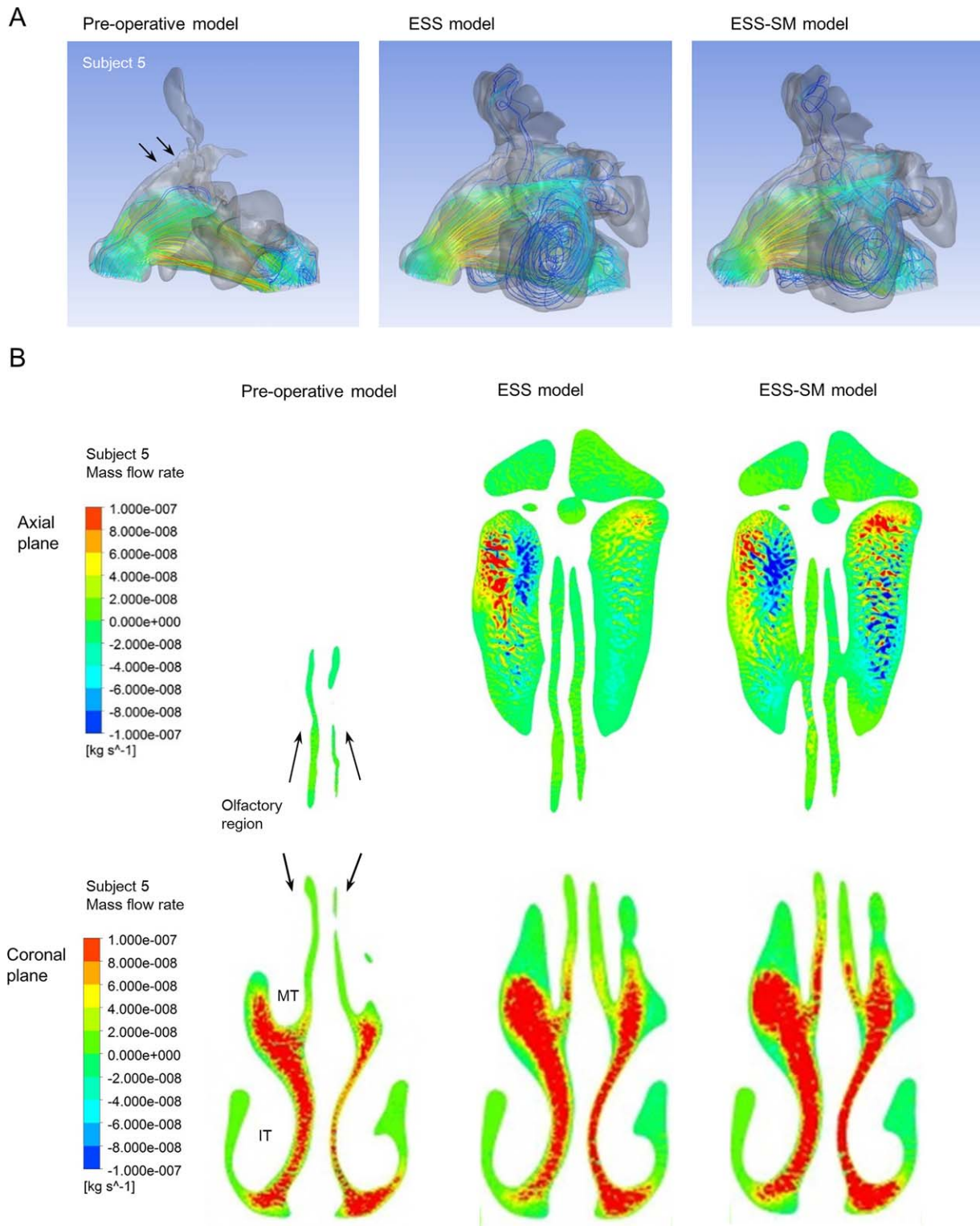


Fig. 8. Streamline and Mass Flow Rate in the Olfactory Region of Chronic Sinusitis Patients. A) Streamline in the preoperative model, endoscopic sinus surgery (ESS) that included ethmoidectomy with normal superior meatus model (ESS model), and ESS that included ethmoidectomy with superior meatus enlargement model (ESS-SM model) in the entire nasal cavity. The black arrows indicate the olfactory region. The streamline around the olfactory region is higher in the ESS-SM model than in the other models. B) The mass flow rate in the pre-operative model, ESS model, and ESS-SM model in the axial and coronal planes. The black arrows indicate the olfactory region. Axial plane analysis identified airflow in the upward direction (green, yellow, and red) and downward direction (blue). The mass flow rate in both directions is higher in the ESS-SM model than in the ESS model. MT = middle turbinate; IT = inferior turbinate.

On the other hand, the airflow velocity, streamlines, and mass flow rate in the olfactory region were not different between pre-surgery and the ESS models. This may be because even though the total airflow resistance in the nasal cavity decreased after ethmoidectomy, the increased airflow passed through the middle meatus to the choana and not through the olfactory cleft (Fig. 5), probably because the airflow resistance through the olfactory region does not change with simple ethmoidectomy. On the other hand, virtual removal of the nasal polyps in the cases of chronic sinusitis increased airflow in the olfactory region after ESS (Figs. 7 and 8). This suggests that the post-operative improvement in olfaction with ESS in the clinical setting^{1,2} might be due to the release of the airflow block by nasal polyps and/or mucosal swelling in the olfactory cleft.

The present study appears to be the first to apply ParaView for virtual endoscopy and observe a virtually operated nasal cavity. Nasal CFD combined with virtual surgery has been used in many studies, especially those involving nasal airway obstruction in relation to septoplasty and inferior turbinate reduction.^{6–11} However, few studies have applied this methodology for the investigation of a sinus surgery procedure.^{12,22} One reason of this might be that editing tools available for medical images limit the surgeon's ability to accurately transcribe each operative procedure. Additionally, manual editing of 2D cross-sections can sometimes lead to errors because the surgeon cannot easily evaluate the outcome of editing in familiar 3D views.⁸ The ParaView software used in this study enabled observation of the nasal cavity model in familiar endoscopic views with wide angles as virtual endoscopy, enabling virtual surgery to easily reflect the predicted results of the proposed geometry.

When considering the surgical technique for the superior meatus, it is important to determine whether the olfactory mucosa is removed when enlarging the superior meatus. The human olfactory epithelium appears to be distributed above and below the anterior middle turbinate insertion, and the location is more anterior than previously assumed.¹⁷ The olfactory mucosa was preserved after enlargement of the superior meatus in the present study, and ample margins of the superior insertion of the middle turbinate were present. However, attention should be paid to prevent damage to the olfactory mucosa in clinical settings.

The present study has several limitations. First, only steady inspiratory, resting laminar nasal airflow was considered in the present study. Airflow has been shown to be primarily laminar for resting flow rates in healthy noses;^{23,24} however, turbulent components may be involved in olfactory airflow, especially in the case of sniffing. Therefore, other conditions, such as expiratory flow and sniffing, should be evaluated in future studies. Second, the models used in the first analysis were prepared from subjects without sinusitis. We used CT images from normal subjects because our current focus was to compare airflow after the "most successful" ESS (without any mucosal lesion) with that after ESS-SM in the same subject. This comparison could be easily performed with editing of the normal geometry models. Airflow analysis of the olfactory region with polyps will not

provide much information, as airflow streamlines in the olfactory region are missing in CFD when the space is occupied with polyps.⁴ However, in the second analysis of patients with chronic sinusitis, we found the same trend of postoperative airflow, suggesting that ESS-SM would be effective in actual patients. Futures studies should include the actual postoperative CT images of patients who have undergone ESS. Finally, although our study suggested that ESS-SM increases the airflow in the olfactory region, it remains unclear if ESS-SM provides optimal postoperative airflow for olfaction. Olfaction is affected by many factors, such as the diffusion effects of odorants, transfer of odorant molecules to the olfactory receptors, and severity of mucosal and eosinophilic inflammation (pathological aspect). Therefore, an increase in olfactory airflow does not necessarily indicate better olfactory function, and we need to be careful in considering the clinical implications of our results. Further prospective studies are necessary to investigate if the olfactory airflow difference between surgical techniques is reflected in the difference in postoperative olfaction in clinical settings.

CONCLUSION

Our virtual simulation study suggested that ESS-SM might be an effective procedure for the improvement of postoperative olfactory function, as it increases olfactory airflow. We successfully used an innovative approach involving virtual ESS, virtual endoscopy, and CFD to assess postoperative outcomes after ESS.

ACKNOWLEDGMENTS

We thank Ms. Kae Yamazaki (ANSYS, Japan) and Ms. Yasuko Shiraiishi (Materialise, Japan) for their technical assistance, and Dr. Natsumaro Kutsuna and Dr. Seiichiro Hasezawa (University of Tokyo and LPixel Inc., Japan) for their helpful suggestions.

BIBLIOGRAPHY

1. Baradaranfar MH, Ahmadi ZS, Dadgarnia MH, et al. Comparison of the effect of endoscopic sinus surgery versus medical therapy on olfaction in nasal polyposis. *Eur Arch Otorhinolaryngol* 2014;271:311–316.
2. Briner HR, Jones N, Simmen D. Olfaction after endoscopic sinus surgery: long-term results. *Rhinology* 2012;50:178–184.
3. Miwa T, Uramoto N, Tsukatani T, Furukawa M. Middle turbinate fenestration method: a new technique for the treatment of olfactory disturbance due to chronic sinusitis. *Chem Senses* 2005;30:i214–i215.
4. Zhao K, Pribitkin EA, Cowart BJ, Rosen D, Scherer PW, Dalton P. Numerical modeling of nasal obstruction and endoscopic surgical intervention: outcome to airflow and olfaction. *Am J Rhinol* 2006;20:308–316.
5. Keyhani K, Scherer PW, Mozell MM. Numerical simulation of airflow in the human nasal cavity. *J Biomech Eng* 1995;117:429–441.
6. Frank-Ito DO, Kimbell JS, Laud P, Garcia GJ, Rhee JS. Predicting post-surgery nasal physiology with computational modeling: current challenges and limitations. *Otolaryngol Head Neck Surg* 2014;151:751–759.
7. Rhee JS, Cannon DE, Frank DO, Kimbell JS. Role of virtual surgery in preoperative planning: assessing the individual components of functional nasal airway surgery. *Arch Facial Plast Surg* 2012;14:354–359.
8. Rhee JS, Pawar SS, Garcia GJ, Kimbell JS. Toward personalized nasal surgery using computational fluid dynamics. *Arch Facial Plast Surg* 2011;13:305–310.
9. Wexler D, Segal R, Kimbell J. Aerodynamic effects of inferior turbinate reduction: computational fluid dynamics simulation. *Arch Otolaryngol Head Neck Surg* 2005;131:1102–1107.
10. Kim SK, Na Y, Kim JI, Chung SK. Patient specific CFD models of nasal airflow: overview of methods and challenges. *J Biomech* 2013;46:299–306.
11. Leong SC, Chen XB, Lee HP, Wang DY. A review of the implications of computational fluid dynamic studies on nasal airflow and physiology. *Rhinology* 2010;48:139–145.

12. Di MY, Jiang Z, Gao ZQ, Li Z, An YR, Lv W. Numerical simulation of airflow fields in two typical nasal structures of empty nose syndrome: a computational fluid dynamics study. *PLoS One* 2013;8:e84243.
13. Zhao K, Jiang J, Pribitkin EA, et al. Conductive olfactory losses in chronic rhinosinusitis? A computational fluid dynamics study of 29 patients. *Int Forum Allergy Rhinol* 2014;4:298–308.
14. Garcia GJ, Bailie N, Martins DA, Kimbell JS. Atrophic rhinitis: a CFD study of air conditioning in the nasal cavity. *J Appl Physiol (1985)*2007;103:1082–1092.
15. Nomura T, Ushio M, Kondo K, Yamasoba T. Effects of nasal septum perforation repair surgery on three-dimensional airflow: an evaluation using computational fluid dynamics. *Eur Arch Otorhinolaryngol* 2015;272:3327–3333.
16. Kimbell JS, Garcia GJ, Frank DO, Cannon DE, Pawar SS, Rhee JS. Computed nasal resistance compared with patient-reported symptoms in surgically treated nasal airway passages: a preliminary report. *Am J Rhinol Allergy* 2012;26:e94–98.
17. Leopold DA, Hummel T, Schwob JE, Hong SC, Knecht M, Kobal G. Anterior distribution of human olfactory epithelium. *Laryngoscope* 2000;110:417–421.
18. Féron F, Perry C, McGrath JJ, Mackay-Sim A. New techniques for biopsy and culture of human olfactory epithelial neurons. *Arch Otolaryngol Head Neck Surg* 1998;124:861–866.
19. Ishikawa S, Nakayama T, Watanabe M, Matsuzawa T. Flow mechanisms in the human olfactory groove: numerical simulation of nasal physiological respiration during inspiration, expiration, and sniffing. *Arch Otolaryngol Head Neck Surg* 2009;135:156–162.
20. Zhao K, Scherer PW, Hajiloo SA, Dalton P. Effect of anatomy on human nasal air flow and odorant transport patterns: implications for olfaction. *Chem Senses* 2004;29:365–379.
21. Croce C, Fodil R, Durand M, et al. In vitro experiments and numerical simulations of airflow in realistic nasal airway geometry. *Ann Biomed Eng* 2006;34:997–1007.
22. Wofford MR, Kimbell JS, Frank-Ito DO, et al. A computational study of functional endoscopic sinus surgery and maxillary sinus drug delivery. *Rhinology* 2015;53:41–48.
23. Hahn I, Scherer PW, Mozell MM. Velocity profiles measured for airflow through a large-scale model of the human nasal cavity. *J Appl Physiol (1985)*1993;75:2273–2287.
24. Chung SK, Son YR, Shin SJ, Kim SK. Nasal airflow during respiratory cycle. *Am J Rhinol* 2006;20:379–384.